Results in Physics 26 (2021) 104346

Contents lists available at ScienceDirect

Results in Physics

journal homepage: www.elsevier.com/locate/rinp

A correlational study: Establishing the link between quantum parameters and particle dynamics around Schwarzschild black hole

Muhammad Saeed [a], Israr Ali Khan [b,c,*], Amir Sultan Khan [c], Shah Qasim Jan [d], Saeed Islam [b], Saleh S. Alarfaji [e], Aijaz Rasool Chaudhry [f]

[a] College of Nuclear Science and Engineering, East China University of Technology, Nanchang 330013, China
[b] Department of Mathematics, Abdul Wali Khan University, Mardan, KPK, Pakistan
[c] Institute of Numerical Sciences, Kohat University of Science and Technology, Kohat, KPK, Pakistan
[d] Department of Physics, Quaid-i-Azam University, Islamabad, Pakistan
[e] Department of Chemistry, College of Science, King Khalid University, Abha 61413, P.O.Box 9004, Saudi Arabia
[f] Department of Physics, College of Science, University of Bisha, Bisha 61922, P.O.Box 334, Saudi Arabia

ARTICLE INFO

Keywords:
Quantum corrected-Schwarzschild black hole
Noether symmetries
Conservation laws
Exact equation of motions

ABSTRACT

The field of point particle dynamics is correlated with the study of particle dynamics around the black hole and one can initiate the study of a more complex motion of extended/celestial bodies. In this article, we consider the study of the dynamics of the neutral/charged particles around the quantum corrected-Schwarzschild black hole and Schwarzschild black hole. We investigate Noether symmetries and their conservation laws corresponding to the quantum corrected-Schwarzschild spacetime. We also study the effect of angular momentum, quantum parameters and magnetic field on the dynamics of neutral and charged particles around the quantum corrected-Schwarzschild black hole and Schwarzschild black hole.

1. Introduction

Studies concerning the dynamics of particles (massless/massive) around black hole (BH) have become an interesting field of research for astrophysicists in recent times. Such studies provide us with a better explanation of the geometry of spacetime. Among the studied quantities that are taken into account in this regard, energy and momentum are the most significant ones, as their definitions are based on so many investigations in general relativity. Different attempts are made to explore the momentum and energy of the particles in the presence of dark energy around a BH. Dark energy has been dubbed with different names in various attempts, like the hidden energy, dark energy, cosmological constant and vacuum energy in the existing literature. The observational evidence shows that the necessary ingredient required for the continuously expanding universe is cosmological constant. The momentum and energy of the charge carrying particle around BH in the presence of magnetic field have already been explored [1–3], for example, by employing Janis-Newman-Winicour (JNW) spacetime algorithm, the dynamics of charge particle in the presence of weakly magnetized BH and Schwarzschild (Sch.) BH have been explored in [4–6]. Such studies help in understanding curvature corresponding to gravitational fields in the surrounding of a BH experimentally in comparison with observational data. The study related to momentum and energy of the particle around BH has already been explored in the literature [7–10]. Similarly, a modified version of the Sch. [11] metric was proposed by Kazakov and Solodukhin in 1994. The suggested expression for the metric coefficient according to their study was of the form: $\frac{-2M}{r}+\frac{1}{r}\int^{r}U(\rho)d\rho$, with M being the BH mass. To derive an expression for an empty space, they put $U(\rho)=1$, however, due to quantum fluctuations of the vacuum [12], the term $U(\rho)$ takes the form: $U(\rho)=e^{-\rho}[e^{-2\rho}-\frac{4}{\pi}G_R]^{-1/2}$, where $G_R=G_N ln(\mu/\mu_0)$, G_N is known as the Newton's gravitational constant, $\mu=\mu_0$ represents a scale parameter. So, the metric function for the Schwarzschild (Sch) BH gets the form: $f(r)=[-2M+\sqrt{r^2-a^2}]/r$, where the dimension of quantum correction parameters is that of length upon which the curvature of spacetime is dependent, and $a^2=4G_r/\pi$, with constraint with the radial coordinate is such that $r>a$.

Thus, based on the scenario discussed, we investigate the effect of quantum parameter on the dynamics of neutral as well as charged particle around Schwarzschild BH. We calculate the Noether symmetries with exact conservation laws along with the thermal stability of the QSc (Quantum Corrected Schwarzschild) BH spacetime. We also investigate

* Corresponding author at: Institute of Numerical Sciences, Kohat University of Science and Technology, Kohat 26000, KPK, Pakistan.
E-mail address: israrali@kust.edu.pk (I.A. Khan).

https://doi.org/10.1016/j.rinp.2021.104346
Received 30 December 2020; Received in revised form 24 April 2021; Accepted 15 May 2021
Available online 26 May 2021

the equations of motion (neutral/charged) by taking into account Noether symmetries and calculate of the energy and momentum corresponding to the particle motion in the innermost stable circular orbits (ISCO) and describe the effect of the quantum parameters, angular momentum and magnetic field on the effective potential (U_{eff}), effective force (F_{eff}) and escape velocity (V_{es}) of a neutral and charged particle moving around BH. We will also analyze the said effect graphically. Further, we study the corresponding effect on the orbit's stability of a particle around BH with the help of Lyapunov exponent.

The organization of work in the current paper is such that in Section 2, we study the Noether symmetries for QSc. BH. In Section 3, analysis of particle's dynamics by taking into consideration U_{eff}, F_{eff} and V_{es} is provided. In Section 4, we study the charged particle motion and discuss the behaviour of U_{eff}, F_{eff} and V_{es} of a particle moving around BH having the magnetic field. Conclusion is considered in the last section.

2. Neother symmetries and their conservations laws

Emmy Noether proposed a well know concept that there is a one-to-one correspondence between Noether symmetries and their respective conservation laws studied in [13–16]. The following section entails the said attributes corresponding to the QSc. BH.

2.1. Quantum corrected-Schwarzschild BH

Corresponding to the QSc. BH solution, the expression of the line element [17–19] can be written as:

$$ds^2 = \left(\frac{\sqrt{r^2-a^2}}{r} - \frac{2M}{r}\right)dt^2 - \left(\frac{\sqrt{r^2-a^2}}{r} - \frac{2M}{r}\right)^{-1} dr^2 - r^2(d\theta^2 + sin^2\theta d\phi^2), \tag{1}$$

M defines the mass of BH, a represents the quantum parameter. The corresponding geodesic Lagrangian of (1) is

$$\mathscr{L} = \left(\frac{\sqrt{-a^2+r^2}}{r} - \frac{2M}{r}\right)\dot{t}^2 - \left(\frac{\sqrt{-a^2+r^2}}{r} - \frac{2M}{r}\right)^{-1} \dot{r}^2 - r^2(\dot{\theta}^2 + sin^2\theta\dot{\phi}^2). \tag{2}$$

In order to work out Noether symmetries for the case concerned, first, we will define the symmetries generator as:

$$Y^1 = \xi_\rho \frac{\partial}{\partial s} + \eta^i \frac{\partial}{\partial x^i} + \eta^i_s \frac{\partial}{\partial \dot{x}^i}, \quad i = 0, 1, 2, 3, \tag{3}$$

the symmetry generator defined in (3) expresses the first order prolongation of

$$Y = \xi \frac{\partial}{\partial s} + \eta^i \frac{\partial}{\partial x^i}. \tag{4}$$

By Noether theorem, Y represents the Noether symmetry if it satisfies

$$Y\mathscr{L} + (\mathscr{D}\xi)\mathscr{L} = \mathscr{D}A, \tag{5}$$

where $\mathscr{D}$ denotes the differential operator defined by

$$\mathscr{D} = \frac{\partial}{\partial s} + \dot{x}^i \frac{\partial}{\partial x^i}. \tag{6}$$

The term A represents the gauge function, which gives the missing information in the conservation laws related to each Noether symmetry.

The system defined in (5) gives the following solutions:

$$\begin{aligned} &A = K_2, \quad \eta^0 = K_3, \\ &\eta^1 = 0, \quad \eta^2 = -K_5 cos\phi + K_6 sin\phi, \\ &\eta^3 = K_4 + \frac{cos\theta(K_5 sin\phi + K_6 cos\phi)}{sin\theta} \\ &\xi^0 = K_1. \end{aligned} \tag{7}$$

Along with the Noether symmetry generators

$$\begin{aligned} &Y_1 = \frac{\partial}{\partial t}, \quad Y_2 = \frac{\partial}{\partial s}, \quad Y_3 = \frac{\partial}{\partial \phi}, \\ &Y_4 = cos\phi \frac{\partial}{\partial \theta} - cot\theta sin\phi \frac{\partial}{\partial \phi}, \\ &Y_5 = sin\phi \frac{\partial}{\partial \theta} + cot\theta cos\phi \frac{\partial}{\partial \phi}. \end{aligned} \tag{8}$$

The following equation may be used to examine the conservation laws related to the symmetries defined in (7).

$$\psi = \frac{\partial \mathscr{L}}{\partial \dot{x}^i}(\eta^i - \xi\dot{x}^i) + \xi\mathscr{L}? - A. \tag{9}$$

We calculate the symmetry for Y_1. Using the symmetry $\xi = 0$ and $\eta^0 = 1$ in (2), we obtain

$$\frac{\partial \mathscr{L}}{\partial \dot{t}} = 2\left(\frac{\sqrt{r^2-a^2}}{r} - \frac{2M}{r}\right)\dot{t},$$

using these values in (9) we get

$$\psi_1 = 2\left(\frac{\sqrt{-a^2+r^2}}{r} - \frac{2M}{r}\right)\dot{t}(1-0) + 0 - 0 = 2\left(\frac{\sqrt{-a^2+r^2}}{r} - \frac{2M}{r}\right)\dot{t}.$$

In Table 1, the Noether symmetry Y_1 corresponds to the energy and shows that the energy of spacetime is conserved. Likewise Y_2 corresponds to the Lagrangian defined in (2) of the spacetime. Similarly, Y_3 corresponds to angular momentum, and Y_4 as well as Y_5 show the conservation of the corresponding angular momentum. It is shown that the symmetry of the Lagrangian in our case is spherical, that's why it may be mentioned here that the Lie algebra of Killing vector fields corresponds to the Lie group $SO(3)$, which is intrinsically admitted by the corresponding spacetime. It is equally pertinent to note that static spacetime always admits a time-like Killing vector field defined in (8). Similarly, we investigate other conservation laws. The conservation laws related to the symmetries defined in (7) are given in the table as follows:

2.2. Thermal stability

The expression for the line element corresponding to the equation already defined in equ. (1) as:

$$ds^2 = \zeta(r)dt^2 - \zeta(r)^{-1} \times dr^2 - r^2(d\theta^2 + sin^2\theta d\phi^2),$$

Table 1
Conservation laws.

Gen	First integrals
Y_1	$\psi_1 = 2\left(\frac{\sqrt{r^2-a^2}}{r} - \frac{2M}{r}\right)\dot{t}$
Y_2	$\psi_2 = -\left(\left(\frac{\sqrt{r^2-a^2}}{r} - \frac{2M}{r}\right)\dot{t}^2 - \left(\frac{\sqrt{r^2-a^2}}{r} - \frac{2M}{r}\right)^{-1}\dot{r}^2 - r^2(\dot{\theta}^2 + sin^2\theta\dot{\phi}^2)\right)$
Y_3	$\psi_3 = -2r^2 sin^2\theta\dot{\phi}$
Y_4	$\psi_4 = -2r^2(cos\phi\dot{\theta} - cot\theta sin\phi\dot{\phi})$
Y_5	$\psi_5 = -2r^2(sin\phi\dot{\theta} + cot\theta cos\phi\dot{\phi})$

where $\zeta(r) = \left(\frac{\sqrt{r^2-a^2}}{r} - \frac{2M}{r}\right)$. The following equation guarantees coordinate singularity.

$$\left(\frac{\sqrt{r^2-a^2}}{r} - \frac{2M}{r}\right) = 0, \tag{10}$$

solving (10) for r, we obtain

$$r_* = \sqrt{a^2+4M^2} \tag{11}$$

There is a possibility for a positive definite solution only if $r > r_*$. The coordinate at $r = r_*$ with period is defined as:

$$\beta = 4\pi r_*. \tag{12}$$

However, if $r \gg r_*$ then normalization of the killing vector toward 1 is obtained. The inverse of the above period provides information to calculate the temperature to infinity. Employing Tolman law, a localized observer will be able to note the local temperature T by taking a self gravitating system as $g_{11}^{-\frac{1}{2}}$, in the equilibrium position [20]. In this regard, the expression of proportionality constant can be written as:

$$T_\infty = \frac{1}{\beta} = (4\pi r_*)^{-1}. \tag{13}$$

The surface area $A_w = 4\pi r_w^2$ and the Wall temperature T_w are given by York [21]. The hot flat space having T_w (uniform temperature) behaves as a topologically regular solution to the EFEs along with these constraints, whereas the Sch. metric is another solution. If there exists a BH with horizon $r_* < r_w$, then in such a case, the Wall temperature satisfying Tolman law takes the form as:

$$T_w = (4\pi r)^{-1}\left(1 - \frac{r_*}{r_w}\right). \tag{14}$$

This equation is solved for r_w in terms of T_w. The r_* has no positive real root if $r_w T_w < \frac{\sqrt{27}}{8\pi}$. For any value of r_w and T_w, the entropy of BH solution to Eq. (14) is $S = \pi r_*^2$. Additionally, the expression of the solution to the constant surface of the heat capacity may be written as:

$$C_A = T_w \frac{\partial S}{\partial T_w}|_{Aw} = -2\pi r_*^2\left(1 - \frac{r_*}{r_w}\right)\left(1 - \frac{3r_*}{2r_w}\right)^{-1}. \tag{15}$$

We shall have a positive heat capacity and locally thermally stable equilibrium if $r_* < r_w < \frac{3r_*}{2}$.

3. Neutral particle's dynamics

This section pertains to the neutral particle dynamics around the QSc. BH defined in (1). The corresponding angular momentum L with energy E is defined as:

$$E = \left(\frac{\sqrt{r^2-a^2}}{r} - \frac{2M}{r}\right)\dot{t},$$

$$L^2 = \left(r^2 v_\perp + \frac{L_z^2}{sin^2\theta}\right),$$

where

$$v_\perp = r^2\dot{\theta}^2, \quad \dot{x}^\mu \dot{x}_\mu = 1. \tag{16}$$

The approximate expression for the motion of neutral particle may be obtained by introducing the normalization condition defined already in (16),

$$\dot{r}^2 = E^2 - \left(\frac{\sqrt{r^2-a^2}-2M}{r}\right)\left(1 + \frac{L_z^2}{r^2 sin^2\theta}\right). \tag{17}$$

Using $\dot{r} = 0$, and $\theta = \frac{\pi}{2}$, the U_{eff} can be calculated as:

$$E^2 = \left(\frac{\sqrt{r^2-a^2}-2M}{r}\right)\left(1 + \frac{L_z^2}{r^2}\right) = U_{eff}. \tag{18}$$

where U_{eff} is the neutral particle's effective potential with the local minima of a circular orbit at r. Generally, the corresponding angular momentum and energy to local minima are respectively defined as:

$$L_{z_0}^2 = \frac{a^2 r + 2Mr\sqrt{r^2-a^2}}{2r^2 - 3a^2 - 6M\sqrt{r^2-a^2}},$$

$$E_0^2 = \frac{(r\sqrt{r^2-a^2} - 6M\sqrt{r^2-a^2} - 3a^2 + 2r^2)(\sqrt{r^2-a^2}-2M)}{r^2\sqrt{r^2-a^2}}.$$

Now, if the particle collides with another particle at ISCO, then there are chances for the particles to: (i) stay bound in the grip of BH (ii) move towards the grip of BH and, (iii) escape away from BH. Later on, at infinite separation the particle becomes static and behaves like a freely falling body. As a result, it is based on the process of collision. Due to some partial change in the angular momentum and energy of the particle revolving in orbit changes slightly but remains bounded. Rather than the particle can move away or towards BH. To simplify this situation, the particle has a new value of angular momentum, energy, and total angular momentum. It simplifies the whole situation as the azimuthal angular momentum is not changed, while initial radial velocity will be the same after the collision. But energy is changed due to which we analyze the particle's motion. After the collision, the particles get the V_{es} in the equatorial plane in an orthogonal direction. Hence the U_{eff} becomes

$$E^2 = \left(\frac{\sqrt{r^2-a^2}-2M}{r}\right)\left(1 + \frac{(L_z + rv_\perp)^2}{r^2}\right) = U_{eff}. \tag{19}$$

The reason why before collision, the particle's energy is less than this energy is that after the collision the particle provides some energy to the revolving particle. Using (19), we define the V_{es} as follows:

$$v_\perp = \pm\left(\frac{E^2 - \left(\frac{\sqrt{r^2-a^2}-2M}{r}\right)}{\left(\frac{\sqrt{r^2-a^2}-2M}{r}\right)}\right)^{\frac{1}{2}} - \frac{L_z}{r}. \tag{20}$$

3.1. Effective potential

The section deals with the study and comparison of the behaviour of the U_{eff} of the neutral particle along with the illustration of the constraints on the energy of the particle in order to control its dynamics during motion or moving it to ∞ from the vicinity of Sch. BH and QSc. BH. It is important to know that if the case is $a = 0$ then the QSc. BH becomes Sch. BH [7–9]. Fig. 1 shows the nature of the particle moving in radial coordinates having various values of L_z and quantum parameter a. We observed a maximum U_{eff} as angular momentum increases, which shows the existence of a strong repulsion around BH versus $1 < r < 4$, while it decreases and vanishes for a minimum angular momentum and a significant value of radial coordinates. This behaviour of the U_{eff} is in agreement with neutral particle dynamics [7]. Upon examination of Fig. 1, it can also be seen that there is a minimum U_{eff} at $a = 1$, while it increases and becomes maximum as quantum corrected parameters decreases and zero, respectively. Hence it is clear that variation in angular momentum and quantum corrected parameter in radial

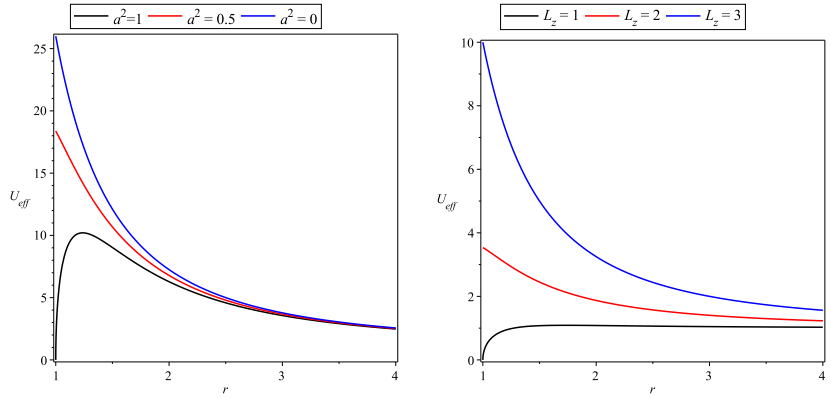

Fig. 1. Comparison plots of U_{eff} of the neutral particles versus the radial coordinates for $r = r/2M, L_z = 1$ (left figure), while $a = 1$ (right figure).

coordinates brings about the same amount of variation in the maxima and minima of U_{eff} of a neutral particle around BH. It may also be noted that there exists a maximum effective potential around Sch. BH as compared to QSc. BH, which clearly implies that there is a strong attraction around QSc. BH.

3.2. Effective force

Effective force is defined by

$$F_{eff} = -\frac{1}{2}\left(\frac{2M\sqrt{-a^2+r^2}+a^2}{r^2\sqrt{-a^2+r^2}}\right)\left(\frac{L_z^2}{r^2+1}\right)+\left(\frac{\sqrt{r^2-a^2}-2M}{r}\right)\left(\frac{L_z^2}{r^3}\right). \tag{21}$$

We consider the motion of the neutral particle around the QSc. BH, where a motion of the particle towards singularity is controlled by gravitational (attractive/repulsive) forces of the scalar vector tensor field [23]. In Fig. 2, we compare the F_{eff} on the neutral particle around QSc. BH versus r for different values of the angular momentum and quantum corrected parameter a. We conclude from Fig. 2 that initially, there is a strong attraction on a particle towards singularity, but it decreases when angular momentum increases as for $L_z = 3$ compared with $L_z = 2, 1$ in the radial interval $(0, 1.5)$. Similarly, the effective force on the neutral particle towards singularity decreases and increases versus different values of quantum corrected parameter a. From Fig. 2, it is also clear that the F_{eff} on the neutral particle becomes attractive at $a = 1$ and becomes repulsive at $(a = 0.5, 0)$. We summarized that there is a minimum F_{eff} on the particle around QSc. BH, which shows a strong attraction around BH while the F_{eff} increases and becomes repulsive around Sch. BH. So, it is concluded that the quantum parameter a decreases the effective force on the particle and increases the attraction towards singularity around BH.

3.3. Escape velocity

The trajectory plots of escape velocity for different cases of angular momentum and quantum corrected parameter with respect to r is shown in Fig. 3. It is clear from the figure that it is difficult for the particle to escape from the grip of BH at large values of the angular momentum, and vice versa. Also, the large value of quantum corrected parameters increases the chance of escaping as shown in Fig. 3. Overall, it may be concluded that the strong angular momentum decreases the chance of escaping, while a large value of quantum corrected parameter increases the chance of escaping for the neutral particle from the vicinity of BH.

4. Charged particle's dynamics

This section deals with the analysis of charged particle dynamics around the QSc. BH already defined in (1). Suppose that at spatial infinity around BH, there exists static, axisymmetric and homogenous magnetic field ($\mathbf{B}$), and let its presence cast an effect on the dynamics of a charged particle around BH. To use the methodology defined by Aliev et al. [24], we established the magnetic field. By employing the metric already defined in (1), we obtained the general killing vector [25–27] i. e.

$$\Box\xi_\mu = 0, \tag{22}$$

where ξ_μ shows the killing vector. Putting (22) for 4-potential A^μ in the Maxwell equation using Lorentz gauge $A^\mu_{;\mu} = 0$, we obtained

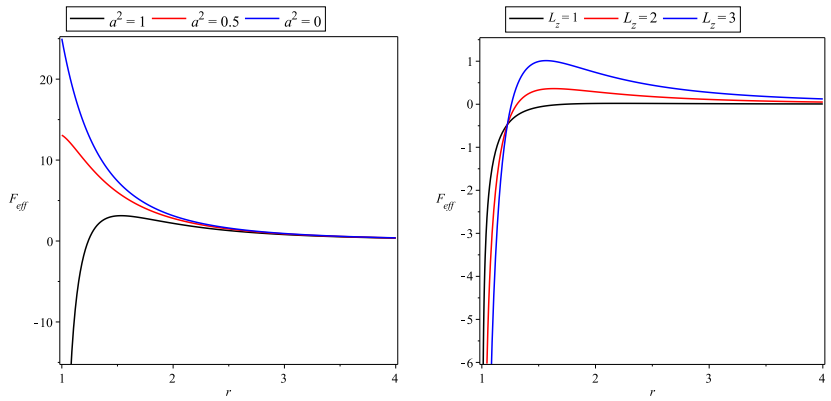

Fig. 2. Comparison plots of F_{eff} of the neutral particle versus the radial coordinates for $r = r/2M, L_z = 1$ (left figure), while $a = 1$ (right figure).

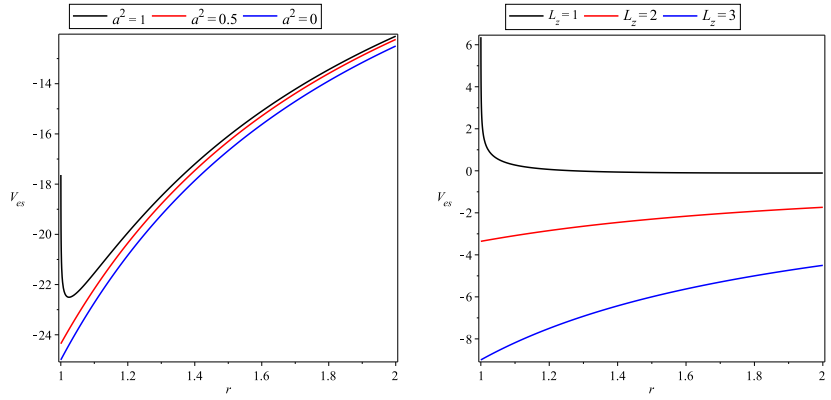

Fig. 3. Comparison plots of V_{es} of the neutral particle versus the radial coordinates for $r = r/2M, L_z = 25$ (left figure), while $a = 1$ (right figure).

$$A^{\mu} = \frac{\mathbf{B}}{2}\xi^{\mu}_{(\phi)}. \tag{23}$$

The killing vector relating to 4-momentum that is invariant under the symmetry may be written as:

$$L_{\xi}A_{\mu} = A_{\mu,\nu}\xi^{\nu} + A_{\nu}\xi^{\nu}_{,\mu} = 0. \tag{24}$$

Using the magnetic field vector [6]

$$\mathbf{B}^{\mu} = -\frac{1}{2}e^{\mu\nu\lambda\sigma}F_{\lambda\sigma}u_{\nu}, \tag{25}$$

where $e^{\mu\nu\lambda\sigma} = \frac{\epsilon^{\mu\nu\lambda\sigma}}{\sqrt{-g}}$, $\epsilon_{0123} = 1, g = det(g_{\mu\nu})$ and $\epsilon^{\mu\nu\lambda\sigma}$ is Levi–civita symbol. Maxwell's tensor is

$$F_{\mu\nu} = A_{\mu,\nu} - A_{\nu,\mu}. \tag{26}$$

Utilizing the metric defined in (1) for a static local observer, we get

$$u^{\mu}_{0} = \left(\frac{\sqrt{r^2 - a^2} - 2M}{r}\right)^{-\frac{1}{2}}\xi^{\mu}_{t}, \quad u^{\mu}_{3} = (rsin\theta)^{-1}\xi^{\mu}_{(\phi)}. \tag{27}$$

At $\dot{r} = 0$, which is also called as the turning point, the rest of the component reduces to zero. By working out equations as given in (23) and (25), we get:

$$\mathbf{B}^{\mu} = \mathbf{B}\left(\frac{\sqrt{r^2 - a^2} - 2M}{r}\right)^{-\frac{1}{2}}\left(cos\theta\delta^{\mu}_{r} - \frac{sin\theta\delta^{\mu}_{\theta}}{r}\right). \tag{28}$$

The direction of magnetic field for the case concerned is alone $z-axis$, and for this reason we take $\mathbf{B} > 0$. For a curved spacetime, the Lagrangian of moving particle [29] is written as:

$$\mathscr{L} = \frac{1}{2}g_{\mu\nu}u^{\mu}u^{\nu} + \frac{qA_{\mu}}{m}u^{\mu}. \tag{29}$$

In the above equation m represents the mass, while q represent the charge of the revolving particle. The generalized 4-momentum of particles are:

$$P_{\mu} = qA_{\mu} + mu_{\mu}. \tag{30}$$

The expression for the new constant of motion can be written as:

$$\dot{t} = \frac{rE}{\left(\sqrt{r^2 - a^2} - 2M\right)}, \quad \dot{\phi} = \frac{L_z}{r^2 sin^2\theta} - B, \tag{31}$$

where $B = \frac{q\mathbf{B}}{2m}$. Using these constraints in (2), r and θ takes the form

$$\ddot{\theta} = \frac{sin2\theta(L_z^2 - B^2)}{r^4 sin^4\theta} - \frac{2\dot{r}\dot{\theta}}{r}, \tag{32}$$

$$\ddot{r} = \frac{E^2(-a^2 - M\sqrt{r^2 - a^2})}{(r^2 - a^2 - 2M\sqrt{r^2 - a^2})} + \frac{\dot{r}^2(-a^2 - M\sqrt{-a^2 + r^2})}{(r^2 - a^2 - 2M\sqrt{r^2 - a^2})} + r\left(\frac{\sqrt{-a^2 + r^2} - 2M}{r}\right)\left(\dot{\theta}^2 + sin^2\theta(\frac{(L_z)}{r^2 sin^2\theta} - B)^2\right) - 2sin^2\theta(\frac{(L_z)}{r^2 sin^2\theta} - B)(\frac{L_z}{rsin^2\theta}). \tag{33}$$

Also, using the normalization condition, $\dot{x}^{\mu}\dot{x}_{\mu} = 1$, we have

$$E^2 = \dot{r}^2 + r^2\left(-\frac{2M}{r} + \frac{\sqrt{-a^2 + r^2}}{r}\right)\dot{\theta}^2 + \left(-\frac{2M}{r} + \frac{\sqrt{r^2 - a^2}}{r}\right)\left(1 + r^2 sin^2\theta\left(\frac{L_z}{r^2 sin^2\theta} - B\right)^2\right). \tag{34}$$

4.1. Effective potential

The U_{eff} of the charged particle orbiting around BH in the equatorial plane can be written as:

$$U_{eff} = \left(-\frac{2M}{r} + \frac{\sqrt{r^2 - a^2}}{r}\right)\left(1 + r^2\left(\frac{L_z}{r^2} - B\right)^2\right). \tag{35}$$

Fig. 4 presents the U_{eff} plots of the charged particle with respect to radial co-ordinates for different magnetic field B and quantum corrected parameter a. The U_{eff} at $a = 1$ is minimum at $r = 1$, and at $a = 0.5, r = 0.7$ but as radial co-ordinates increase it moves towards the maximum. Hence, due to the large value of quantum corrected parameters, the particle is less likely to achieve orbit stability. Similarly, it can also be seen in the figure that, initially, there is low U_{eff} at $B = 0$ compared with $B = 1, 1.5$ respectively. It is interesting to note that U_{eff} moving away from the horizon is minimum for a weaker magnetic field B. The width of the ISCO, however, shows a decreasing trend for a stronger magnetic field. This phenomenon is in agreement with the results [3,24,28]. Therefore, we can observe that the strong magnetic field and the quantum parameter increase the stability of orbit; otherwise, it decreases, and the particle either heads towards BH or it escapes to infinity. Also, there is a maximum effective potential around Sch. BH as compared to QSc. BH, which shows that there exists a strong attraction around QSc. BH as compared to Sch. BH.

The differentiation of (35) with respect to r yields,

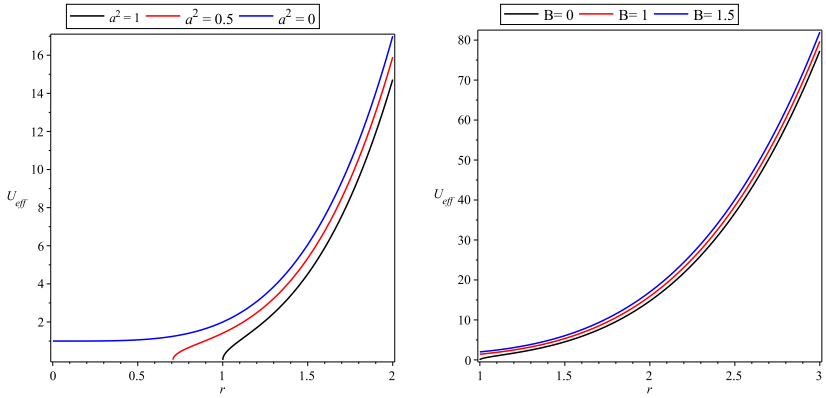

Fig. 4. Comparison plots of U_{eff} of the charged particle versus the radial coordinates for $r = r/2M, L_z = 1$ (left figure), while $a = 1$ (right figure).

$$\frac{dU_{eff}}{dr} = \left(\frac{-a^2 - 2M\sqrt{r^2 - a^2}}{r^2\sqrt{r^2 - a^2}}\right)\left(1 + r^2\left(\frac{L_z}{r^2} - B\right)^2\right) - 2\left(\frac{-2M + \sqrt{-a^2 + r^2}}{r}\right)\left(\frac{L_z^2}{r^3} - rB^2\right). \tag{36}$$

4.2. Effective Force

The F_{eff} on the charged particle around BH is defined as:

$$F_{eff} = -\frac{1}{2}\frac{dU_{eff}}{dr} = -\frac{1}{2}\left(\frac{-2M\sqrt{r^2 - a^2} - a^2}{r^2\sqrt{r^2 - a^2}}\right)\left(1 + r^2\left(\frac{L_z}{r^2} - B\right)^2\right) + \left(\frac{\sqrt{-a^2 + r^2} - 2M}{r}\right)\left(\frac{L_z^2}{r^3} - rB^2\right). \tag{37}$$

The plot pattern of F_{eff} with respect to different values of B and a is shown in Fig.5. It can be seen that the F_{eff} decreases when field strength has a maximum value as compared to minimum values, which shows that magnetic field increases the grip of BH versus small radial co-ordinates but for large radial co-ordinates, the particle escapes away from BH which becomes constant. Fig. 5 also explains the nature of F_{eff} on a particle versus quantum corrected parameter a. We observed that the F_{eff} on a particle decreases as the quantum corrected parameter increases. We concluded that there is a minimum F_{eff} on the particle around QSc. BH, which shows that there exists a strong attraction around the said BH, whereas the F_{eff} increases and becomes repulsive around Sch. BH. So, it is concluded that the quantum parameter a decreases the effective force on the particle and increases the attraction towards singularity around BH.

4.3. Escape velocity

Using $\theta = \frac{\pi}{2}$ and $\dot{r} = 0$, the U_{eff} in the magnetic field B after the collision is defined:

$$E^2 = U_{eff} = \left(\frac{\sqrt{r^2 - a^2}}{r} - \frac{2M}{r}\right)\left(1 + r^2\left(\frac{(L_z + v_\perp r)}{r^2} - B\right)^2\right). \tag{38}$$

The V_{es} of the particle gets the form

$$v_\perp = \pm\left(\left(\frac{rE^2 - \left(\sqrt{r^2 - a^2} - 2M\right)}{\left(\sqrt{r^2 - a^2} - 2M\right)}\right)^{\frac{1}{2}} + rB\right) - \frac{L_z}{r}. \tag{39}$$

The expression for the angular variable already defined in (31) is

$$\dot{\phi} = \frac{L_z}{r^2 sin^2\theta} - B. \tag{40}$$

It is evident that for the attractive nature of the Lorentz force, the left-hand side of the above equation becomes negative [29] and vice versa. This implies that the sense of motion for the charged particle near BH is clockwise. Additionally, the effect of a strong magnetic field on a charged particle is more than that of a weaker one. Consequently, we observed that the escaping power of V_{es} for the particle from ISCO increases for a weak magnetic field. We also consider the behaviour of the V_{es} for various values of the magnetic field B and quantum corrected parameter a in Fig.6 graphically. The V_{es} of a particle around BH increases in the existence of a significant value of quantum parameter a, and it creates more chances for a particle to escape from the grip of BH.

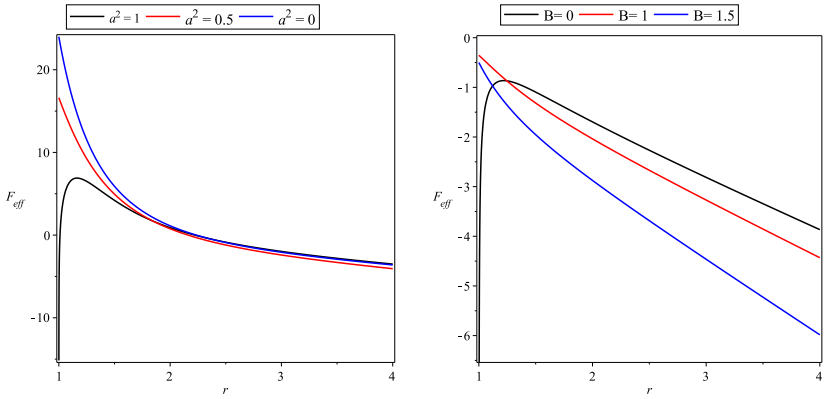

Fig. 5. Comparison Plots of F_{eff} on the charged particle versus the radial coordinates for $r = r/2M, L_z = 1$ (left figure), while $a = 1$ (right figure).

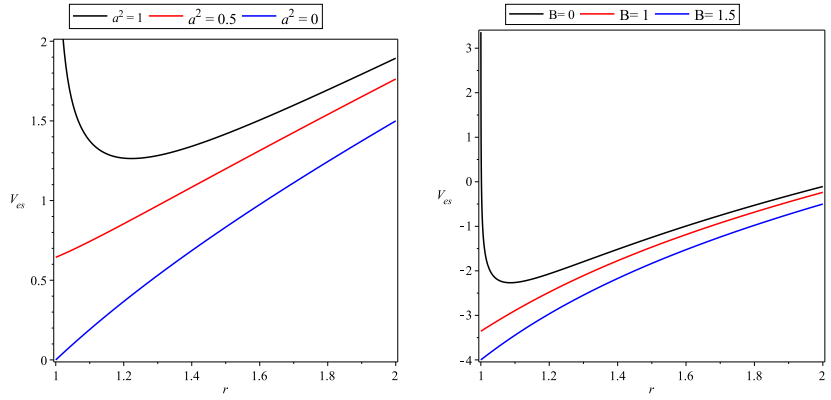

Fig. 6. Comparison plots of V_{es} of the charged particle versus radial coordinates for $r = r/2M, L_z = 25$ (left figure), while $a = 1$ (right figure).

In Fig. 6, we also studied V_{es} versus B, and it is observed that there exists an inverse relationship between escape velocity of the particle and the strength of the magnetic field, i.e. when the field is weak, the escape velocity is higher and vice versa.

5. Conclusion and observations

In this article, a comparative study of the neutral as well as charged particle's dynamics is provided by taking into account into QSc. BH versus Sch. BH. Calculations of Noether symmetries along with their respective conservative laws followed by an investigative effort regarding the constraints on thermal stability is carried out in Section 2.1 and 2.2, respectively. Considering the dynamics of a neutral particle, both the effective potential and effective force around QSc. BH are observed to portray a strongly decreasing trend versus large radial co-ordinate as compared to that around Sch. BH. At the same time, the escape velocity of the particle was found to have an increasing behaviour around QSc. BH in comparison with Sch. BH. In consideration of the dynamics of the charged particle, it is observed that the effective force of the charged particle decreases versus large radial co-ordinates having a strong magnetic field, and is observed to have an attractive nature, which shows that there is a strong attraction around QSc. BH as compared to Sch. BH. Meanwhile, the escape velocity, in this case, is noted to be exactly the same as that of neutral particle. It is additionally found that the chance for a particle to escape from the grip of BH may be directly correlated with the quantum parameter and magnetic field. Overall; it is observed that the quantum parameter affects the particle motion and is of key importance in the accelerated motion of the particle towards singularity around BH.

Declaration of Competing Interest

The authors declare that they have no known competing financial interests or personal relationships that could have appeared to influence the work reported in this paper.

Acknowledgement

The authors from Saudi Arabia extend their appreciation to Deanship of Scientific Research at King Khalid University for funding the work through Research Project (R.G.P. 1/214/41).

References

[1] Mishra KN, Chakrabotry DK. Orbits of a charged particle in a skew uniform magnetic field on kerr back ground geometry. Astrophys Space Sci 1999;260(441).
[2] Teo E. Gen Relativ Gravit 2003;35:1909.
[3] Hussain S, Hussain I, Jamil M. Dynamics of a charged particle around a slowly rotating Kerr black hole immersed in magnetic field. Eur Phy J C 2014;74:3210.
[4] Babar GZ, Jamil M, Lim YK. Dynamics of a charged particle around a weakly magnetized naked singularity. Int J Mod Phys D 2016;25:1650024.
[5] Pugliese D, Quevedo H, Ruffni R. Circular motion of neutral test particles in Reissner-Nordström spacetime. Phys Rev D 2011;83:104052.
[6] Zahrani AMA, Frolov VP, Shoom AA. Synchrotron radiation from a weakly magnetized Schwarzschild black hole. Phys Rev D 2013;87:084043.
[7] Khan IA, Khan AS, Islam S. Dynamic of the particle around de Sitter Schwarzchild black hole surrounded by quintessence. Int J Mod Phys A 2020.
[8] Khan AS, Ali F, Khan IA. Dynamic of the particle around anti de Sitter Schwarzchild black hole environed by quintessence. Phys: Can. J; 2020.
[9] Khan IA, Ali F, Islam S, Khan AS. The role of the cosmological constant in dynamics of the particle in the Schwarzschild black hole. Phys Scr 2020.
[10] Khan IA, Khan AS, Islam S, Jan SQ, Nisar KS, Shah MU. Particle dynamics around quintessential Reissner-Nordström black hole. Results Phys 2021;21:103790.
[11] Kazakov D, Solodukhin S. On quantum deformation of the Schwarzschild solution. Nucl Phys B 1994;429:153.
[12] Kim W, Kim Y. Phase transition of quantum-corrected Schwarzschild black hole. Phys Lett B 2012;718:687.
[13] Noether E, Nachr. Koing. Gesell. Wissen, Gottinngen, Math. Phys. KI. Heft. 1971;2: 186.
[14] Khan IA, et al. Explication of the conserved quantities corresponding to the spacetimes carrying 10 Noether symmetries. Int J Geom Method Mod Phy 2020;18 (4):2150053–215068.
[15] Khan AS, Khan IA, Islam S, Ali F. Noether symmetry analysis for novel gravitational wave-like spacetimes and their conservation laws. Mod Phys Lett A 2020;35(28): 2050234.
[16] Jamal S. Dynamical systems: Approximate Lagrangians and Noether symmetries. Int J Geom Methods Mod Phys 2018.
[17] Konoplya RA. Quantum corrected black holes: Quasinormal modes, scattering, shadows. Phys Lett B 2020:135363.
[18] Bezerra VB, Lobo IP, Graça JM, Luis CS. Effects of quantum corrections on the criticality and efficiency of black holes surrounded by a perfect fluid. Phys J C 2019;79:949.
[19] Shahjalal M. Thermodynamics of quantum-corrected Schwarzschild black hole surrounded by quintessence. Nucl Phys B 2019;940:63.
[20] Prestidge T, Phys. Dynamic and thermodynamic stability and negative modes in Schwarzschild-anti-de Sitter black holes. Phys. Rev. D. 2000;61:084002.
[21] York JW. Black-hole thermodynamics and the Euclidean Einstein action. Phys Rev D 1986;33:2092.
[23] Moffat JW. JCAP 2006;0603:3004.
[24] Aliev AN, Gal'stov DV. Sov Phys Usp 1989;32:75.
[25] Wald RM. Black hole in a uniform magnetic field. Phys Rev D 1974;10:1680.
[26] Aliev AN, Ozdemir NN. Mon Not R Astron Soc 1978;336:241.
[27] Landau LD, Lifshiz EM. The Classical Theory Of Fields. Oxford: Pergamon Press; 1975.
[28] Khan AS, Ali F. The dynamics of particles around time conformal AdS-Schwarzschild black hole. Phys Dark Universe 2019;19:100389.
[29] Frolov VP, Shoom AA. Motion of charged particles near a weakly magnetized Schwarzschild black hole. Phys Rev D 2010;82:084034.